AIMS Mathematics, 10(10): 24446–24468.
DOI: 10.3934/math.20251084
Received: 10 July 2025
Revised: 01 October 2025
Accepted: 13 October 2025
Published: 24 October 2025

http://www.aimspress.com/journal/Math

Research article

Analytical solution to linearized groundwater responses in sloping unconfined leaky aquifers under transient surface recharge

Siao-Ya Tang and Ping-Cheng Hsieh*

Department of Soil and Water Conservation, National Chung Hsing University, Taichung 40227, Taiwan

* **Correspondence:** Email: ida364@email.nchu.edu.tw; Tel: +8860422840381; Fax: +8860422876851.

Abstract: The increasing frequency of extreme climate events due to global warming has intensified water scarcity during prolonged droughts, highlighting the urgent need for effective water resource management. In Taiwan, where land availability is limited and population density is high, reservoirs serve as the primary storage mechanism; however, groundwater still accounts for approximately one-third of the total water supply. This study investigates groundwater level responses in a sloping, unconfined, leaky aquifer subjected to transient surface recharge and temporally varying boundary conditions, represented using Heaviside step functions. The governing Boussinesq equation is linearized through a time-dependent averaging strategy to enable analytical tractability, and then solved using the generalized integral transform technique (GITT). A convergence and validity analysis of the linearization is provided to justify this approximation. Model validation is conducted by comparing the analytical results under uniform recharge and horizontal slope conditions with prior benchmark studies. The proposed method demonstrates improved computational efficiency compared with Laplace-transform-based approaches. The findings indicate that steeper aquifer slopes shift peak water levels downslope, hydraulic conductivity controls the drawdown rate, and even small leakage rates exert a significant influence on groundwater dynamics.

Keywords: sloping aquifer; recharge; boundary water level; integral transform; leaky layer
Mathematics Subject Classification: 76S05

1. Introduction

Groundwater plays a critical role in satisfying domestic, agricultural, and industrial water demands, particularly in regions such as Taiwan, where steep topography, short river systems, and seasonally concentrated precipitation limit surface water availability. Despite receiving considerable annual rainfall, Taiwan's per capita water availability remains among the lowest globally. This vulnerability was underscored during the 2021 drought, driven by deficient wet-season rainfall, a lack of typhoons, and anomalous atmospheric patterns. Consequently, groundwater—supplying nearly one-third of Taiwan's total water demand—has become an increasingly dependable resource. However, overextraction has led to serious issues including land subsidence, saltwater intrusion, and declining water quality. Accurate groundwater level estimation is thus essential for sustainable water management and geotechnical safety. However, conventional monitoring via observation wells remains costly, labor-intensive, and spatially constrained.

Extensive research has examined groundwater flow in unconfined aquifers under varying recharge and boundary conditions. Marino [1] analyzed a horizontal unconfined aquifer connecting two rivers with equal water levels and derived analytical solutions under the Dupuit assumption, employing Laplace transforms to evaluate water table fluctuations induced by transient surface recharge. Ram and Chauhan [2] developed an analytical model for one-dimensional unsteady flow in a sloping aquifer with an impermeable base and exponentially varying boundaries, validated through Hele–Shaw experiments. Verhoest and Troch [3] addressed steady-state groundwater levels in sloping aquifers with impermeable lower boundaries, solving the linearized Boussinesq equation via Laplace transforms. Zissis et al. [4] extended this work by comparing analytical and finite-difference numerical solutions under variable recharge and boundary fluctuations, demonstrating that linearization provides accurate results when the dimensionless recharge-to-conductivity ratio is non-negative. In Taiwan, Hung et al. [5] investigated rainfall recharge in multilayer aquifers using sandbox experiments and iterative analytical methods, confirming the method's validity and proposing its extension to confined–unconfined systems. Teloglou and Bansal [6] derived transient analytical solutions for unconfined aquifers with leakage and variable river boundary conditions, validating their results against numerical simulations. Building on this, Bansal [7] further examined the effects of slope and localized transient recharge, finding that increased slope accelerates water table stabilization while reducing its peak height.

Various studies have proposed different methods for linearizing the nonlinear h^2 term in the Boussinesq equation. Hung et al. [8], Bansal [9], and Bansal et al. [10] introduced a direct linearization approach aimed at enhancing accuracy, while Liang and Zhang [11] employed a weighted average of groundwater head values. Hung et al. [12] suggested using the average of the initial and final river boundary levels, adjusted according to the characteristics of each boundary, to approximate the nonlinear term. Although linearization facilitates the analytical treatment of the Boussinesq equation, its accuracy tends to decline under conditions of steep slopes or high recharge. Nonetheless, comparative analyses by Zissis et al. [4] and Hung et al. [12] demonstrated that linearized formulations can still yield acceptable agreement with numerical solutions across a variety of conditions.

Additionally, several analytical solutions have been developed to examine groundwater's responses to the uniform and nonuniform recharge as well as the influence of variable boundary water levels [13–17]. Other researchers have explored the effects of leakage layers on groundwater dynamics [8,18]. For instance, Hung et al. [8] utilized the general solution of Upadhyaya and

Chauhan [19] to derive an analytical expression for groundwater levels, which they successfully validated using experimental data from a sandbox model. Recently, contemporary analytical methods continue to advance the modeling of groundwater dynamics under transient recharge and complex boundary conditions. Upadhyaya and Kankarej [20] provided both analytical and numerical solutions for groundwater level fluctuations under time-varying recharge rates with an exponential function form, offering practical insight into dynamic recharge impacts. Shi et al. [21] derived analytical solutions capturing transient confined–unconfined flow due to pumping in layered aquifers, highlighting dynamic head interactions across contiguous strata. Valois et al. [22] derived an analytical expression for well–aquifer responses to Earth tides, explicitly addressing storage and compressibility in leaky systems. This work demonstrates the feasibility of extending transform-based solutions to include external periodic drivers in aquifer systems, aligning closely with the techniques developed in this paper and reinforcing the relevance of analytical techniques for leaky aquifer modeling. Turnadge and Keery [23] offered analytical and adjoint solutions for cumulative groundwater response in wedge-shaped aquifers, facilitating insights into complex geometric impacts on flow. Recently, fractal geometry has been used to model flow and transport in porous systems with strong heterogeneity. For example, Huang et al. [24] developed a two-scale fractal permeability model for vuggy porous media, showing that void (vug) scale and pore scale both contribute, especially under changing stress, to variations in permeability in carbonate media. Yang et al. [25] applied a rough capillary bundle fractal model to characterize how pore roughness and pore size distribution in dense porous media affect permeability, highlighting the sensitivity of flow to microscopic geometry. More recently, a fractal analytical model for forced imbibition dynamics in shale reservoirs has been proposed [26], which includes nanoscale slip and demonstrates how fractality influences front propagation. These contributions show that fractal methods are actively being used to capture complexity in porous media, which could complement traditional transform or integral technique models in aquifer flow.

Building on prior work, this research introduces a novel linearization strategy that approximates the nonlinear term in the Boussinesq equation by averaging the initial water depth with that from the preceding time step. The governing equation is linearized through a modified formulation based on the methodologies of Bear [27] and Marino [1], and then solved analytically using the generalized integral transform technique (GITT) developed by Özisik [28]. Unlike traditional approaches reliant on Laplace transforms,the generalized integral transform technique (GITT) offers improved flexibility for incorporating time-variable inputs and boundary conditions. The resulting analytical model integrates the aquifer's slope, transient surface recharge, and basal leakage, allowing for the evaluation of spatiotemporal groundwater fluctuations in sloping unconfined, leaky aquifers. This framework enhances computational efficiency and serves as a practical tool for water resource management and geotechnical planning in hydrogeologically complex settings.

2. Methodology

2.1. Establishment of the governing equation

This study derives an analytical solution for groundwater flow in a sloping, unconfined aquifer with basal leakage, subjected to time-variable boundary water levels and transient surface recharge. The aquifer domain extends over a distance L, and a coordinate system is established accordingly, as illustrated in Figure 1.

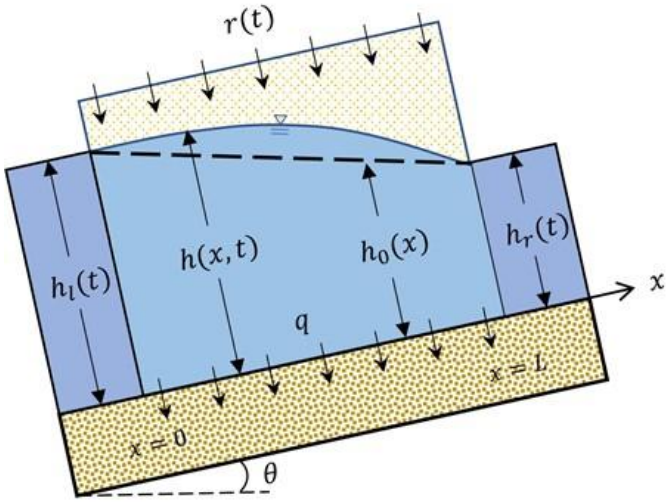

Figure 1. Schematic of a sloping unconfined leaky aquifer.

In the schematic, the water levels in the left and right channels are denoted by $h_l(t)$ and $h_r(t)$, respectively. The surface recharge is applied uniformly over the domain $0 \le x \le L$, and the groundwater level distribution within the aquifer is represented by $h(x,t)$. Here, x is the coordinate [L], t is the time [T], θ: slope angle [-], $h_0 \equiv h_0(x,0)$ is the initial groundwater level distribution [L], r is the surface recharge rate [L/T], S is the specific yield, [-] k is the hydraulic conductivity of the aquifer [L/T], k_s is the hydraulic conductivity of the leakage layer [L/T], q is the unit leakage rate through the bottom [L/T].

The following assumptions are adopted in this study:

(1) The porous medium is composed of incompressible soil particles.
(2) The soil is homogeneous and isotropic.
(3) Capillary rise and evaporation within the aquifer are neglected.
(4) Groundwater flow is laminar and governed by Darcy's law.

The governing equation is derived by integrating the groundwater continuity equation with Darcy's law, following the approach of Childs [29]. For a sloping unconfined aquifer experiencing surface recharge and vertical leakage, the Boussinesq equation takes the following form:

$$\frac{\partial}{\partial x}\left(h\frac{\partial h}{\partial x}\right) - tan\,\theta\,\frac{\partial h}{\partial x} + \frac{r-q}{k\,cos^2\,\theta} = \frac{S}{k\,cos^2\,\theta}\frac{\partial h}{\partial t}, \tag{1}$$

where the leakage rate q is approximated using Darcy's law for vertical flow through a semi-permeable base of thickness b, as follows:

$$q \approx \frac{k_s}{b}[h(x,t) - h_0(x,0)] = \frac{k_s(h-h_0)}{b}. \tag{2}$$

To facilitate analytical treatment, the equation is transformed using h^2 as the primary dependent variable. By multiplying the leakage term numerator and denominator by $h + h_0$, and applying the identity, we have

$$\frac{\partial}{\partial x}\left(h\frac{\partial h}{\partial x}\right)=\frac{1}{2}\frac{\partial^2 h^2}{\partial x^2}.$$

Then Eq (1) becomes

$$\frac{1}{2}\frac{\partial^2 h^2}{\partial x^2}-tan\,\theta\,\frac{1}{2h}\frac{\partial h^2}{\partial x}+\frac{r}{k\,cos^2\,\theta}-\frac{k_s\left(h^2-{h_0}^2\right)}{k\,cos^2\,\theta(h_0+h)b}=\frac{S}{2\,cos^2\,\theta hk}\frac{\partial h^2}{\partial t}. \tag{3}$$

To simplify the nonlinear terms in the denominator, the linearization technique is required, wherein h is replaced by an effective average depth $h'\equiv h'(x,t)$, defined as the mean of the initial groundwater level and the level from the immediately preceding time step, referring to [1] and [24]. Accordingly, Eq (3) becomes

$$\frac{1}{2}\frac{\partial^2 h^2}{\partial x^2}-tan\,\theta\,\frac{1}{2h'}\frac{\partial h^2}{\partial x}+\frac{r}{k\,cos^2\,\theta}-\frac{k_s\left(h^2-{h_0}^2\right)}{k\,cos^2\,\theta(h_0+h')b}=\frac{S}{2\,cos^2\,\theta h'k}\frac{\partial h^2}{\partial t}. \tag{4}$$

Let $\delta^*=k_s/[(h_0+h')kb]$; substituting into Eq (4) yields

$$\frac{1}{2}\frac{\partial^2 h^2}{\partial x^2}-tan\,\theta\,\frac{1}{2h'}\frac{\partial h^2}{\partial x}+\frac{r}{k\,cos^2\,\theta}-\frac{\delta^*\left(h^2-{h_0}^2\right)}{cos^2\,\theta}=\frac{S}{2\,cos^2\,\theta h'k}\frac{\partial h^2}{\partial t}. \tag{5}$$

2.2. Initial and boundary conditions

To solve the linearized Boussinesq equation, appropriate initial and boundary conditions must be defined. These conditions account for both spatial and temporal variability in the groundwater system.

• Initial condition

Prior to the onset of recharge, the groundwater level is assumed to vary linearly between the left and right boundaries, expressed as

$$h(x,0)=h_0(x)=h_l(0)+\frac{h_r(0)-h_l(0)}{L}x, 0<x<L. \tag{6}$$

• Boundary conditions:

The groundwater levels at the left and right boundaries vary with time and are set as

$$h(0,t)\equiv h_l(t), t>0, \tag{7}$$

$$h(L,t)\equiv h_r(t), t>0. \tag{8}$$

The boundary water levels and surface recharge can be represented using the Heaviside step function $u(\eta)$, to capture piecewise-constant time variations:

$$h_l(t)=\sum_{i=1}^{M}h_{li}\,[u(t-t_{i-1})-u(t-t_i)], \tag{9}$$

$$h_r(t)=\sum_{i=1}^{M}h_{ri}\,[u(t-t_{i-1})-u(t-t_i)], \tag{10}$$

$$r(t)=\sum_{j=1}^{N}r_j\,[u\left(t-t_{j-1}\right)-u(t-t_j)]. \tag{11}$$

Here, h_{li} and h_{ri} represent the boundary water levels on the left and right sides, respectively, during

the i-th time interval ($\Delta t_i = t_i - t_{i-1}$), with M denoting the total number of river stage (channel water level) data points. Similarly, r_j denotes the surface recharge rate during the j-th time interval ($\Delta t_j = t_j - t_{j-1}$), and N is the total number of surface recharge data points. Furthermore, $u(\eta)$ denotes the unit step (Heaviside) function, with $u(\eta) = 0$ for $\eta < 0$ and $u(\eta) = 1$ for $\eta \geq 0$. This definition clarifies its role in representing piecewise-constant recharge and boundary conditions.

2.3. Nondimensionalization

To reduce the complexity of the governing equation and generalize the analysis, dimensionless variables are introduced, based on the characteristic scales of the system.

We define the following dimensionless variables:

$$X = \frac{x}{L},\ H = \frac{h^2 - {h_0}^2}{{h_0}^2},\ T = \frac{t}{t_r},\ R = \frac{rt_r}{h_0} \quad (t_r\text{: recharging duration}). \tag{12}$$

To simplify the resulting dimensionless form of the equation, we introduce the following dimensionless parameters:

$$\alpha = \frac{2h'}{h_0 S}, \gamma = \frac{\cos^2\theta h' k t_r}{SL^2}, \xi = \frac{2h' k t_r}{S}\delta^*, \phi = \frac{k t_r \sin 2\theta}{2SL}. \tag{13}$$

The dimensionless groups have clear physical interpretations: α represents the recharge-to-storage ratio, controlling the amplitude of mound formation; γ relates lateral transmissivity, the duration of recharge, and scaling diffusion effects; ξ is the leakage-to-transmissivity ratio, quantifying the intensity of vertical exchange; and ϕ reflects the slope effects on downstream drainage.

Substituting these variables into the linearized governing equation, Eq (5), yields

$$\frac{\partial H}{\partial T} = \gamma \frac{\partial^2 H}{\partial X^2} - \phi \frac{\partial H}{\partial X} + \alpha R - \xi H. \tag{14}$$

The dimensionless initial and boundary conditions become

$$H(X, 0) = H_0(X) = 0, 0 < X < 1, \tag{15}$$

$$H(0, T) = \frac{{h_l}^2 - h_0^2}{{h_0}^2} \equiv H_L(T), T > 0, \tag{16}$$

$$H(1, T) = \frac{{h_r}^2 - h_0^2}{{h_0}^2} \equiv H_R(T), T > 0. \tag{17}$$

This nondimensional framework significantly simplifies the solution process, reduces the parameters' interdependence, and enhances the generalizability of the results across various physical settings.

2.4. Exact solutions

To solve Eq (14) using Özisik's [28] GITT, variable substitution is applied to eliminate the first-order derivatives and the source term of H, transforming the equation into a heat conduction type of form.

The procedure involves

- Applying the variable transformations $H = H_V e^{\frac{\phi X}{2\gamma} + \varsigma T}$ (with $\varsigma = \frac{-3\phi^2}{4\gamma} - \xi$) to simplify Eq (14), which becomes

$$\gamma e^{\varsigma T}\frac{\partial^2 H_V}{\partial X^2}+\alpha Re^{-\frac{\phi X}{2\gamma}}=e^{\varsigma T}\frac{\partial H_V}{\partial T}, \tag{18}$$

with the transformed initial and boundary conditions

$$H_V(X,0)=0,\ 0<X<1, \tag{19}$$

$$H_V(0,T)=H_{VL},T>0, \tag{20}$$

$$H_V(1,T)=H_{VR},T>0. \tag{21}$$

- Converting the boundary conditions to a homogeneous form by defining the following relationship:

$$\begin{aligned}\Delta H_V(X,T)&\equiv H_V(X,T)-\left[H_{VL}(T)+\left(H_{VR}(T)-H_{VL}(T)\right)X\right]\\&=H_V-(1-X)H_{VL}(T)-XH_{VR}(T).\end{aligned} \tag{22}$$

Substituting Eq (22) into Eq (18) yields

$$\gamma e^{\varsigma T}\frac{\partial^2 \Delta H_V}{\partial X^2}=-\alpha Re^{-\frac{\phi X}{2\gamma}}+e^{\varsigma T}\left(\frac{\partial \Delta H_V}{\partial T}+(1-X)\frac{dH_{VL}}{dT}+X\frac{dH_{VR}}{dT}\right), \tag{23}$$

with the corresponding initial and boundary conditions

$$\Delta H_V(X,0)=0,\ 0<X<1, \tag{24}$$

$$\Delta H_V(0,T)=0,\ T>0, \tag{25}$$

$$\Delta H_V(1,T)=0,\ T>0. \tag{26}$$

- Performing the integral transform using an orthogonal kernel $K(\beta_m,X)=\sqrt{2}\,sin(\beta_m X),\ \beta_m=m\pi,\ (m\in \boldsymbol{N})$.

Integral transform:

$$H_T(\beta_m,T)=\int_{X=0}^{1}K(\beta_m,X)\cdot\Delta H_V(X,T)\,\mathrm{d}X. \tag{27}$$

Inverse transform:

$$\Delta H_V(X,T)=\sum_{m=1}^{\infty}K(\beta_m,X)\cdot H_T(\beta_m,T). \tag{28}$$

Applying the integral transform to the partial differential equation (PDE), Eq (23), leads to a first-order ordinary differential equation (ODE) in time

$$\frac{dH_T}{dT}+\gamma{\beta_m}^2H_T+\varepsilon(T)=0, \tag{29}$$

with

$$\varepsilon(T)\equiv\int_{X=0}^{1}K(\beta_m,X)\left[-\alpha Re^{-\frac{\phi X}{2\gamma}}+(1-X)\frac{dH_{VL}}{dT}+X\frac{dH_{VR}}{dT}\right]dX. \tag{30}$$

- Solving for the transformed variable H_T and applying the inverse transform

To solve the ODE, Eq (29), with a zero initial condition, $H_T(T=0)=0$, we can find

$$H_T=-\mathrm{e}^{-\gamma{\beta_m}^2T}\int_0^{T'=T}\varepsilon(T')e^{\gamma{\beta_m}^2T'}dT'. \tag{31}$$

Employing Eq (28) to Eq (31) yields

$$\Delta H_V(X,T) = -\sum_{m=1}^{\infty}\sqrt{2}sin(\beta_m X)\left(e^{-\gamma\beta_m{}^2 T}\int_0^{T'=T}\varepsilon(T')e^{\gamma\beta_m{}^2 T'}dT'\right). \quad (32)$$

- Reconstructing the physical solution $H(X,T)$ from the transformed domain

Applying Eq (22) to Eq (32), we have

$$H_V(X,T) = -\sum_{m=1}^{\infty}\sqrt{2}sin(\beta_m X)\int_0^{T'=T}\varepsilon(T')e^{\gamma\beta_m{}^2(T'-T)}dT' + (1-X)H_{VL}(T) + XH_{VR}(T). \quad (33)$$

Applying variable transformations $H = H_V e^{\frac{\phi X}{2\gamma}+\varsigma T}$ (with $\varsigma = \frac{-3\phi^2}{4\gamma} - \xi$), we can obtain the dimensionless groundwater level

$$H = \sum_{m=1}^{\infty}2sin(\beta_m X)\left\{\int_0^{T'=T}e^{-\gamma\beta_m{}^2(T-T')}\int_{X=0}^{1}sin(\beta_m X)\left(\alpha R e^{\varsigma(T-T')} - \left[(1-X)\left(\frac{dH_L}{dT'} - \varsigma H_L\right) + X\left(\frac{dH_R}{dT'} - \varsigma H_R\right)\right]\right)dXdT'\right\} + (1-X)H_L(T) + XH_R(T). \quad (34)$$

Subsequently, the variable boundary water levels, Eqs. (9)–(10), and the recharge, Eq (11), are also expressed in dimensionless form

$$H_L = \sum_{j=1}^{N} H_{Lj}\left[U\left(T-T_{j-1}\right) - U\left(T-T_j\right)\right], \quad (35)$$

$$H_R = \sum_{j=1}^{N} H_{Rj}\left[U\left(T-T_{j-1}\right) - U\left(T-T_j\right)\right], \quad (36)$$

$$R = \sum_{j=1}^{N} R_j\left[U\left(T-T_{j-1}\right) - U\left(T-T_j\right)\right]. \quad (37)$$

Substituting the above three equations into Eq (34), the physical solution H can be employed in the practical application. This analytical solution captures the spatiotemporal evolution of groundwater levels in sloping, unconfined, leaky aquifers under transient recharge and time-varying boundary conditions. It offers a computationally efficient alternative to fully numerical methods while preserving high fidelity to the governing physics.

2.5. Convergence and validity of the linearization

When the nonlinear Boussinesq equation is simplified by replacing h with the averaged value $h'(x,t)$, a small difference (residual) remains. This residual ($Res(\cdot)$) is roughly proportional to the gap between the true head h and the averaged head h'

$$Res(h) = \frac{\partial}{\partial x}\left[(h-h')\frac{\partial h}{\partial x}\right]. \quad (38)$$

Using the mean value theorem for the function $f(h) = 1/h$, one obtains

$$\left|\frac{1}{h} - \frac{1}{h'}\right| \leq \frac{|h-h'|}{(\min\{h,h'\})^2}. \quad (39)$$

A similar bound holds for $1/(h_0+h)$). Thus, each coefficient replacement introduces an error proportional to $|h-h'|$, and therefore

$$|Res(h)| \leq C|h-h'|, \text{ or } Res(h) = O(|h-h'|), \quad (40)$$

for some constant $C > 0$, depending only on the parameters, and the symbol $O(\cdot)$ describes how large a term can be, relative to some small quantity, as that quantity tends to zero.

Let h be the solution of the original nonlinear problem (Eq (3)) and let h^* be the solution of the linearized problem (Eq (4)). The error is defined as

$$err = h - h^*. \tag{41}$$

Subtracting the two equations gives a diffusion-type inequality of the following form:

$$\frac{\partial(err)}{\partial t} \leq D\frac{\partial(err)}{\partial x} + C|h - h'|, \tag{42}$$

where D is a positive coefficient that comes from the diffusion term of the linearized groundwater equation. Since h' is chosen as a local average over short time steps, the difference $|h - h'|$ scales with the time step size Δt. As a result, the error is bounded by

$$\text{Error size} \leq K^*\Delta t,$$

where K^* is a constant. In other words, as $\Delta t \to 0$, the linearized solution approaches the nonlinear one.

In practice, our numerical experiments confirm this behavior: The series solution using the GITT converges with about 30 terms, while Laplace-transform-based methods often need 50–60 terms for the same accuracy (see Section 3.2). This shows both the validity of the linearization and the efficiency of the proposed method.

3. Results and discussion

On the basis of the analytical solutions derived under assumed boundary and initial conditions, this section presents the results and discusses their physical implications. The variations in groundwater levels are analyzed and compared with previous studies to validate the analytical solution. Subsequently, the influence of different hydraulic conductivities, aquifer slopes, surface recharge types, and boundary conditions on groundwater levels is thoroughly examined.

3.1. Parameterization in numerical simulations

In all simulations, the upstream boundary head (h_l) and the downstream boundary head (h_r) were chosen to represent plausible channel stages at the two ends of the aquifer domain. Their values were set in accordance with earlier benchmark studies (e.g., Bansal [15], [16]) and with typical field-scale head differences observed over 100-m sloping unconfined aquifers. Specifically, h_l was fixed between 5 and 6 m and h_r was 3–4 m, yielding a head difference of about 2 m across the domain, which is consistent with the ranges used for validation in Section 3.2.

The recharge input (r) was selected to represent rainfall-derived infiltration under event conditions. For the constant recharge cases, r was set to approximately 0.004 m/h, in agreement with Bansal [15] and typical storm intensities reported in the hydrogeological literature. For the time-variable cases, three different temporal patterns were applied: early peak, central peak, and double peak. Each profile was scaled so that the total cumulative recharge over the simulation horizon was identical, thereby isolating the effect of recharge timing on the groundwater's response.

These parameter choices ensure that the simulations remain directly comparable with prior benchmark studies, while also reflecting realistic boundary heads and recharge magnitudes for sloping leaky aquifers.

3.2. Model validation

The analytical model is benchmarked against the results of Bansal [15], who investigated transient groundwater responses in sloping unconfined aquifers with constant recharge and fixed boundary conditions. Using consistent parameters and boundary conditions ($\theta = 0°, 3°, 7°, S = 0.2, k = 2.5$ m/h, $L = 100$ m, $r = 0.004$ m/h, $h_l = 5$ m, $h_r = 3$ m), the present study shows strong agreement with Bansal's results. Minor discrepancies near the downstream boundary are attributed to differences in the numerical approximations and boundary condition treatments, confirming the robustness of the proposed solution (Figure 2). Moreover, to illustrate the runtime performance, we compared the GITT and Laplace implementations under identical conditions to those above but selecting $\theta = 3°$ and 100 time steps. On a standard desktop (Intel i7, 3.0 GHz, 16 GB RAM), the GITT's solution with 30 terms required 0.42 seconds, while the Laplace-transform-based series with 60 terms required 1.37 seconds. Thus, implementing the GITT was approximately three times faster, consistent with the reduced number of terms needed for convergence, as discussed in Section 3.3.

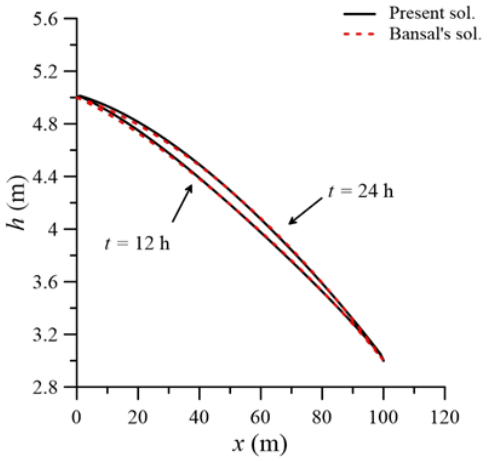

(a) $\theta = 0°,\ k = 2.5$ m/h

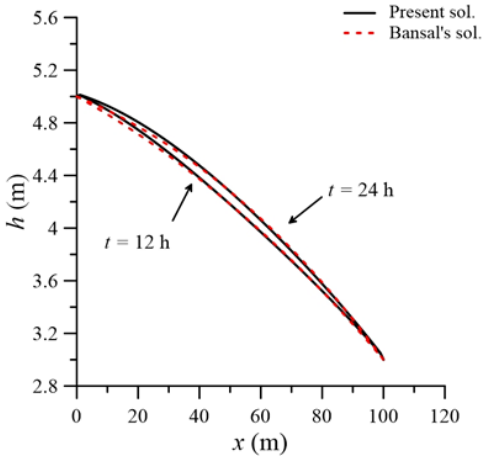

(b) $\theta = 3°,\ k = 2.5$ m/h

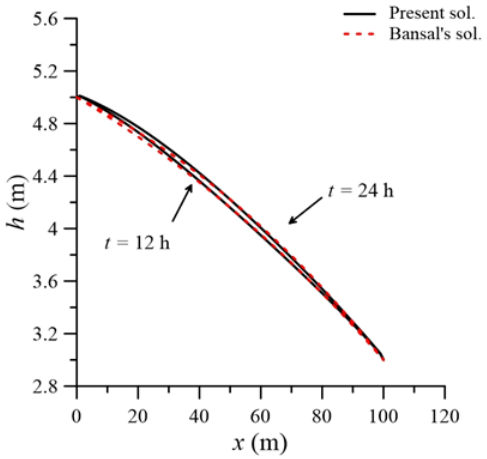

(c) $\theta = 7°,\ k = 2.5$ m/h

Figure 2. Comparison of the present solution with Bansal's solution in 2011.

Although Figure 2 presents a validation for constant recharge with fixed boundaries, this case is a special instance of the general formulation. In our model, recharge and boundary heads are expressed as Heaviside step functions [Eqs. (9)–(11)], which can represent any arbitrary time-varying input as a sequence of constant steps. Because the linearized governing equation is linear in these forcing terms, the accuracy demonstrated for constant recharge directly extends to piecewise-constant and fully time-varying recharge scenarios. Thus, the transient recharge cases analyzed in Sections 3.5 and 3.7 are not extrapolations beyond the validated regime, but belong to the same solution class.

3.3. Convergence behavior of series solutions

Figure 3 compares the convergence behavior of the GITT utilized in this study with that of conventional Laplace transform methods. The present approach demonstrates efficient convergence with approximately 30 terms, in contrast to the 50–60 terms typically needed by Laplace-based solutions. This improvement significantly enhances the computational efficiency, particularly in real-time analyses or large-scale applications where processing resources and time are critical.

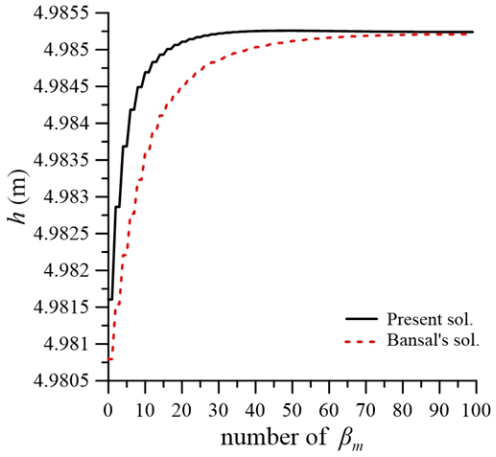

(a) $\theta = 0°,\ k = 2.5$ m/h

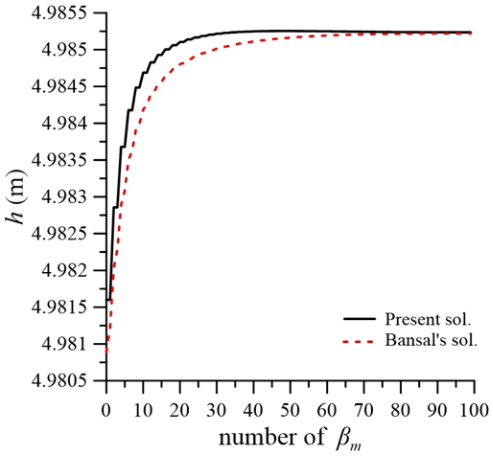

(b) $\theta = 3°, k = 2.5$ m/h

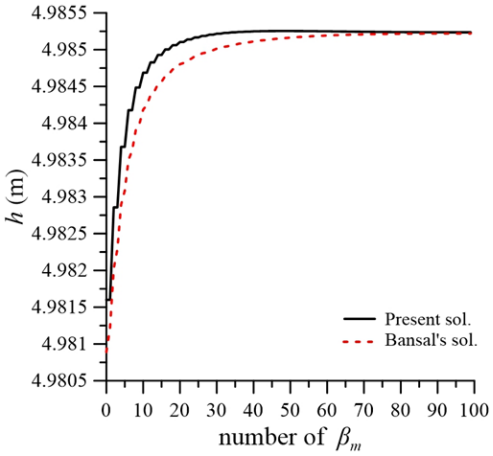

(c) $\theta = 7°, k = 2.5$ m/h

Figure 3. Comparison of solution convergence for the present solution with Bansal's solution in 2011.

3.4. Groundwater responses under uniform recharge

Figure 4 illustrates the groundwater level's distribution under uniform recharge for varying slopes and hydraulic conductivities. Steeper slopes accelerate groundwater flow toward the downstream boundary, leading to reduced water levels. Likewise, higher hydraulic conductivity promotes faster distribution of the recharge water, resulting in lower peak water levels and quicker stabilization. These findings underscore the critical influence of the aquifer's geometry and material properties on recharge efficiency.

3.5. Effects of time-dependent recharge

Three temporal recharge scenarios (early peak, central peak, and double peak) were evaluated under identical cumulative recharge volumes (Figure 5). As illustrated in Figure 6, these scenarios produce distinct groundwater responses. The early peak recharge induces a rapid rise in the groundwater level, followed by a subsequent decline.

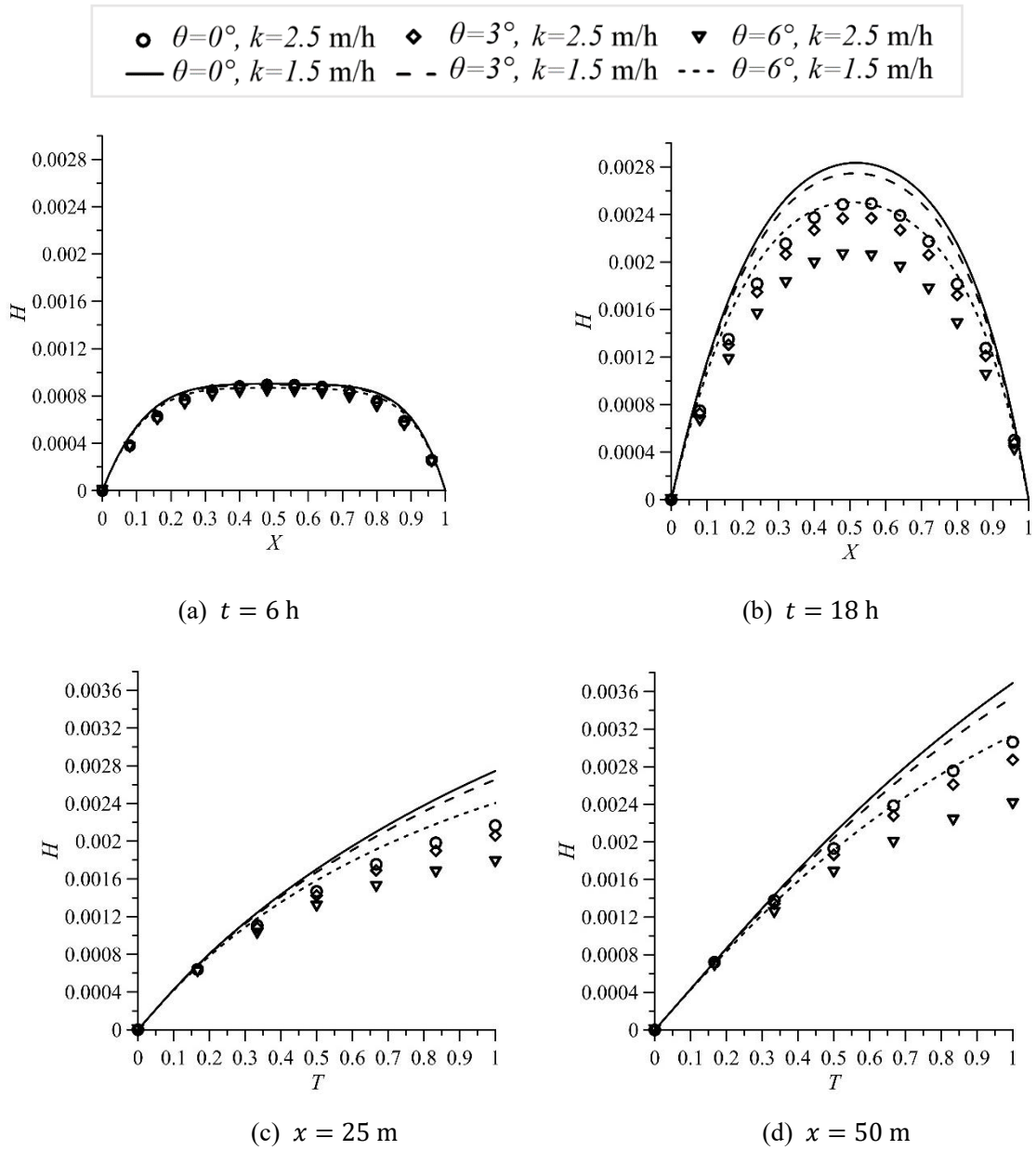

Figure 4. Dimensionless groundwater level distributions for distinct values of θ and k under constant recharge.

In contrast, the central peak and double peak patterns delay the occurrence of peak groundwater levels and sustain elevated levels for longer durations. As the aquifer's slope increases, the location of the peak groundwater level shifts toward the downstream boundary (Table 1), highlighting the interplay between recharge timing and topographic gradient.

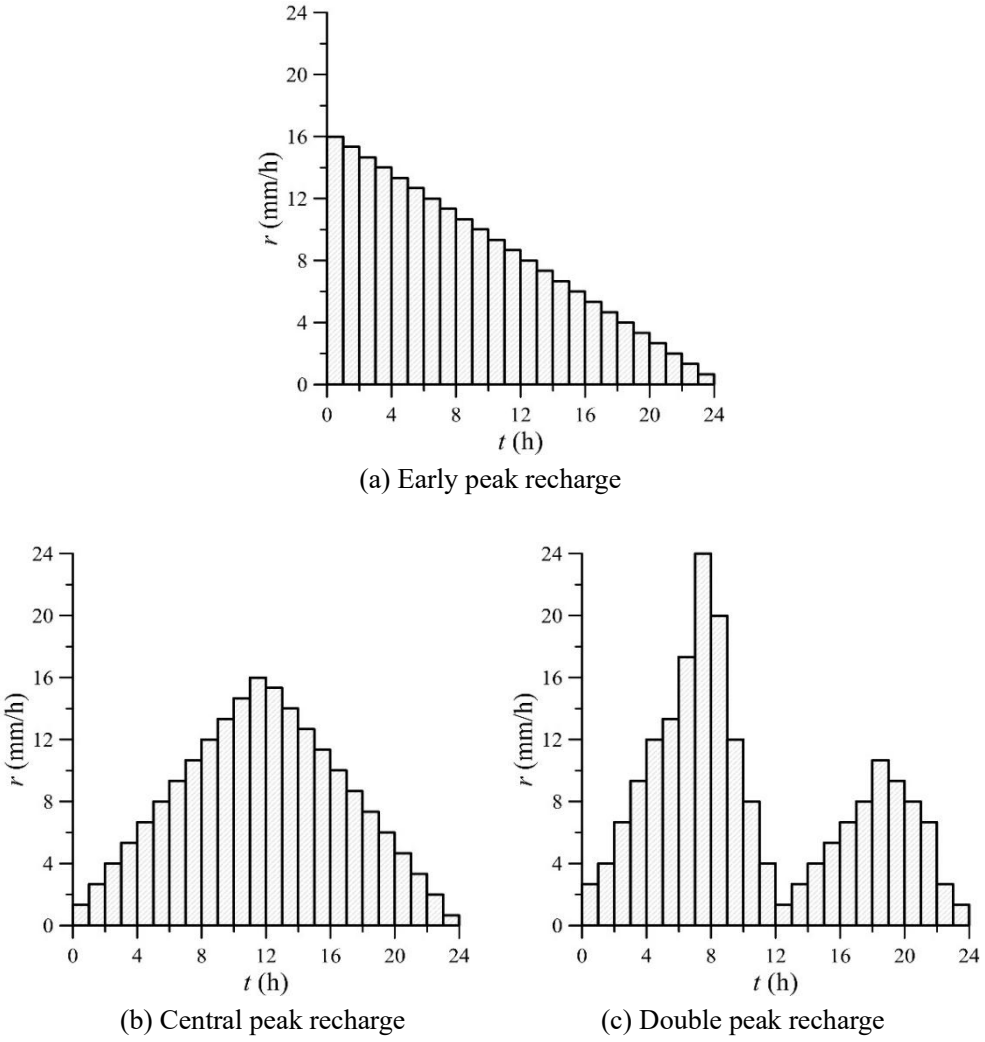

(a) Early peak recharge

(b) Central peak recharge

(c) Double peak recharge

Figure 5. Three types of recharge distributions discussed in this study.

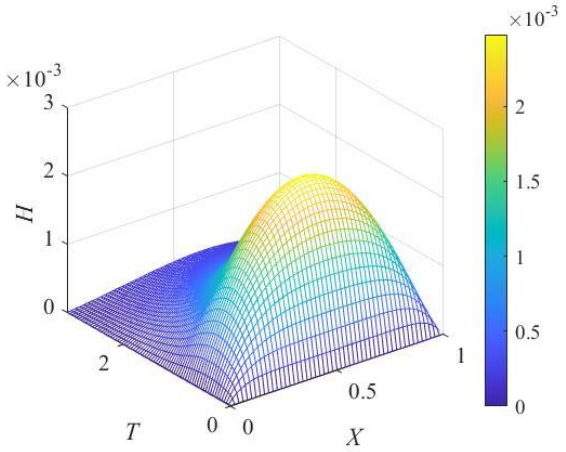

(a) Early peak recharge for $\theta = 0°$

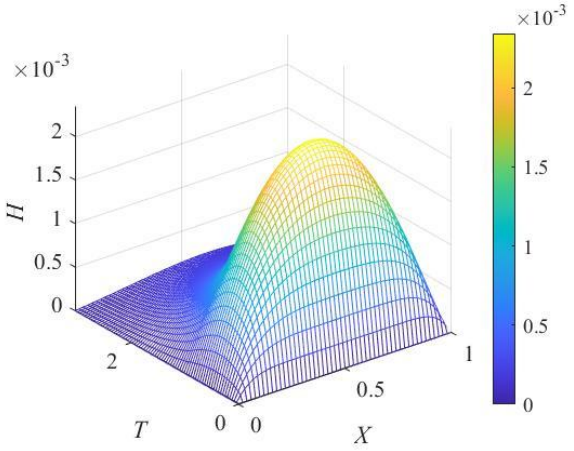

(b) Early peak recharge for $\theta = 3°$

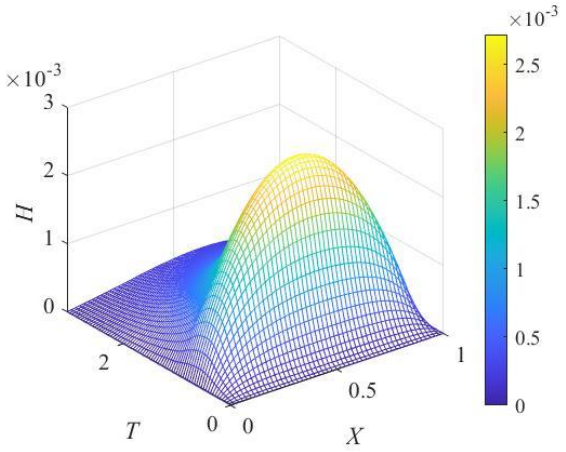

(c) Central peak recharge for $\theta = 0°$

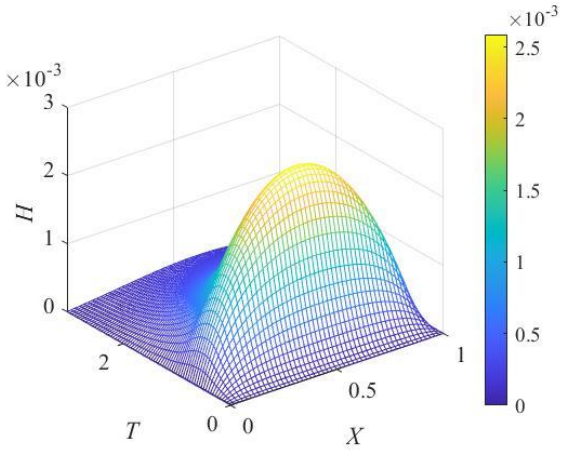

(d) Central peak recharge for $\theta = 3°$

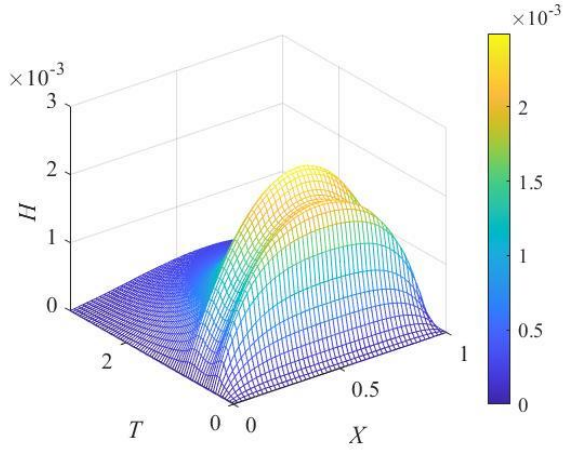

(e) Double peak recharge for $\theta = 0°$

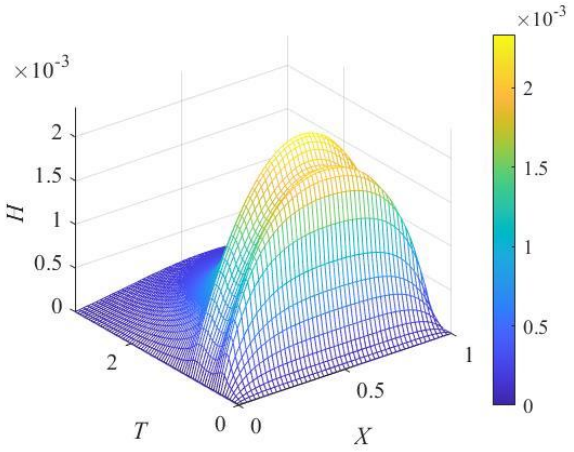

(f) Double peak recharge for $\theta = 3°$

Figure 6. Spatiotemporal variations in dimensionless groundwater levels under distinct recharge types ($k = 2.5$ m/h).

Table 1. Locations and peak values of dimensionless groundwater levels at $t = 12$ h under distinct recharge types for $k = 2.5$ m/h.

Type / θ	Early peak		Central peak		Double peak	
	X	H	X	H	X	H
0°	0.5	0.00221	0.5	0.00148	0.5	0.00216
3°	0.5	0.00213	0.5	0.00145	0.5	0.0021
6°	0.48	0.00192	0.48	0.00135	0.48	0.00194

The spatial profiles at t = 12 h (Figure 6) further demonstrate that higher aquifer slopes shift the groundwater peak closer to the lower boundary, reflecting gravitational effects on the flow direction. The spatiotemporal variations shown in Figure 6 highlight the significant influence of recharge timing on groundwater's distribution. Table 1 quantifies the peak water levels and their corresponding locations under varied slopes and hydraulic conductivities, emphasizing the importance of considering both recharge dynamics and the aquifer's properties in predictive analyses.

3.6. Influence of leakage under uniform recharge

The impact of vertical leakage from underlying strata was assessed under conditions of uniform surface recharge (r = 0.01 m/h) and fixed or linearly increasing boundary water levels. Using representative parameters ($k = 2.5$ m/h, $S = 0.2$, $h_l = 5$ m, $h_r = 3$ m, and $L = 100$ m), the temporal evolution of leakage rates was examined. As shown in Figure 7, under both boundary scenarios, the leakage rate increases as the boundary water levels rise. Additionally, the rate of increase becomes more pronounced over time, indicating that higher boundary water levels not only elevate the magnitude of leakage but also accelerate its temporal progression. These findings underscore the considerable influence of boundary water levels on both the intensity and growth rate of leakage in unconfined leaky aquifers. The observed behavior emphasizes the necessity of accounting for time-varying boundary conditions when evaluating groundwater's flow and leakage dynamics, particularly in systems with semi-permeable basal layers.

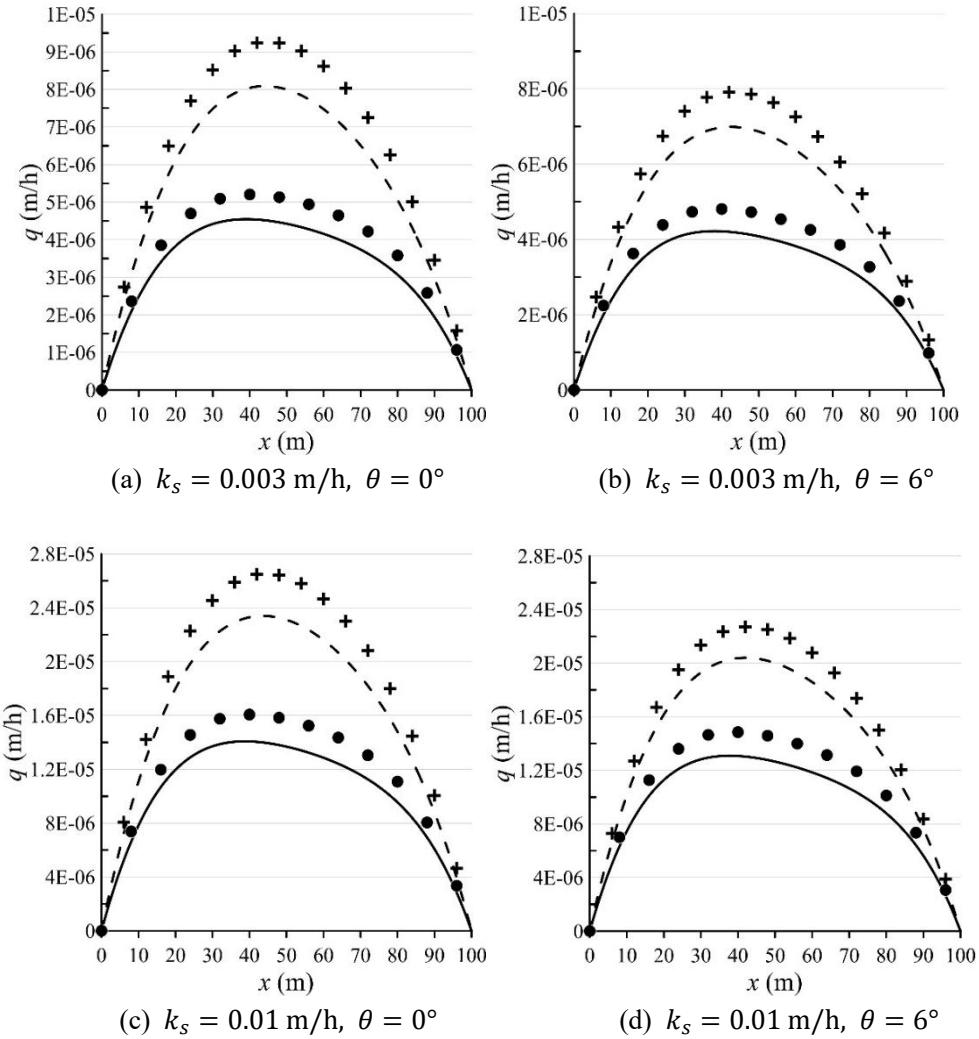

Figure 7. Variation in the leakage rate under uniform recharge and fixed/variable boundary water levels. The solid line and dashed line denote the case of a fixed boundary water level at t =12 h and $t = 24$ h, respectively. The curves with solid circles and plus markers denote the case of a variable boundary water level at $t = 12$ h and $t = 24$ h, respectively.

3.7. Interaction of leakage and time-dependent recharge

To explore the combined effects of vertical leakage and temporal recharge variability, simulations were performed using three types of variable recharge profiles (early peak, central peak, and double peak) at two levels of hydraulic conductivity in the leakage layer ($k_s = 0.003$ and 0.01 m/h). The leakage rates in Figure 8 (for $k = 2.5\ \mathrm{m/h}$) increase with increased leakage layer conductivities across all recharge types, resulting in decreased groundwater levels. Elevated leakage limits the extent of recharge-induced mounding and enhances the relative influence of slope, particularly under steeper gradients. Further analysis in Figure 9 (for $k = 1.5\ \mathrm{m/h}$) reveals that the effect of hydraulic conductivity (k-value) on the leakage rate is significant. As the k-value decreases, groundwater flow is hindered, and more water percolates through the semi-permeable layer so that the leakage rate increases across the three types of variable recharge. The observed variations in leakage rates are primarily attributed to differences in the leakage characteristics (k_s), while the slope's effect diminishes when the recharge pattern is held constant. Nonetheless, slope angle still exerts a minor effect on the observed differences. These results demonstrate that recharge timing and leakage parameters must be jointly considered when modeling transient groundwater. Failure to incorporate the leakage characteristics may lead to overestimations of an aquifer's response and misrepresentations of groundwater dynamics under variable recharge conditions.

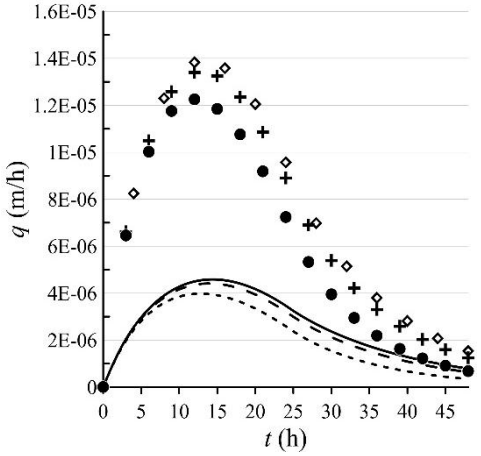

(a) Early peak recharge

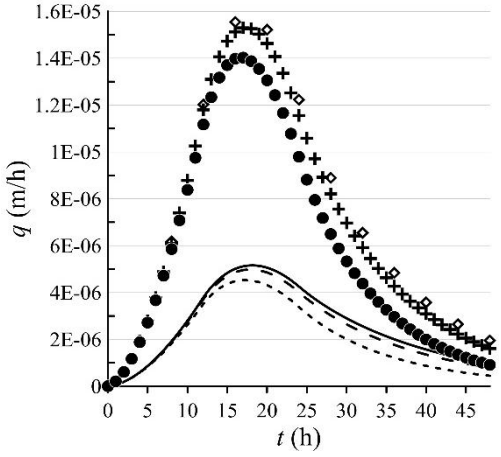

(b) Central peak recharge

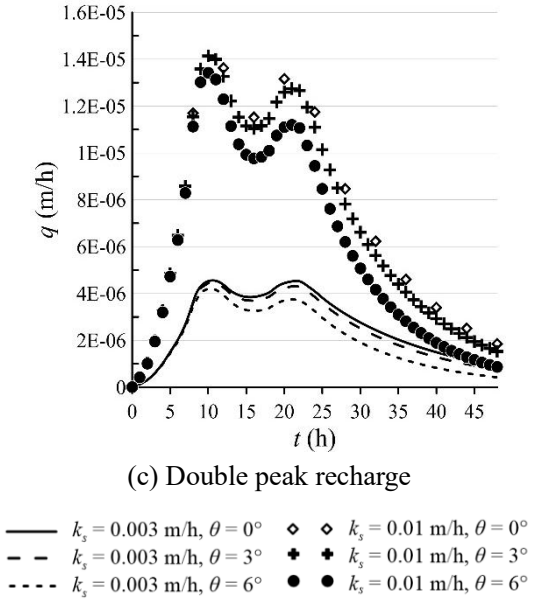

(c) Double peak recharge

Figure 8. Variation in the leakage rate under temporally variable recharge and fixed boundary water levels ($x = 25$ m, $k = 2.5$ m/h).

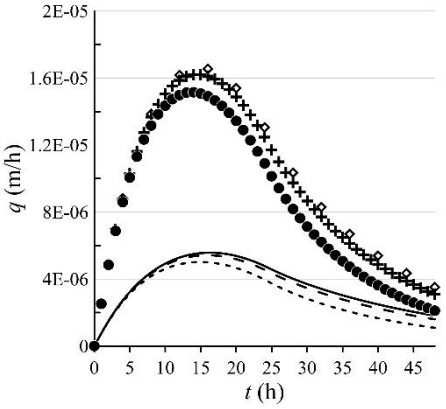

(a) Early peak recharge

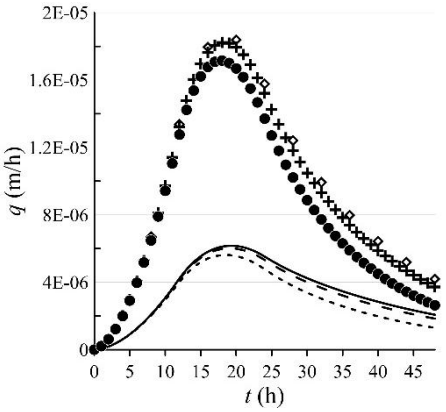

(b) Central peak recharge

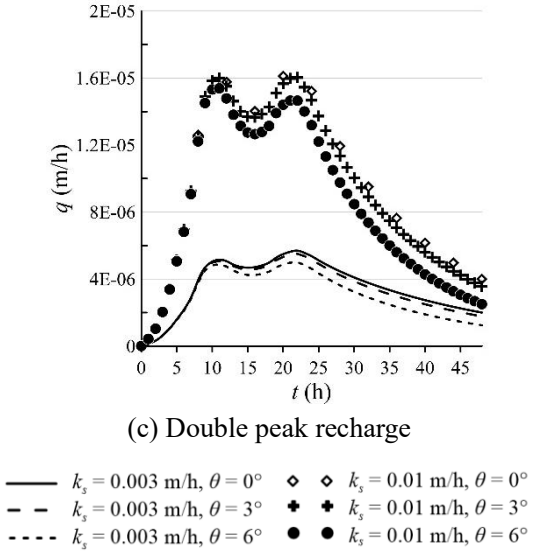

Figure 9. Variation in the leakage rate under temporally variable recharge and fixed boundary water levels ($x = 25$ m, $k = 1.5$ m/h).

4. Conclusions

This study investigates the transient behavior of groundwater in sloping, unconfined leaky aquifers subjected to temporally variable surface recharge and boundary water levels. The governing equation, derived from the Boussinesq equation of [29] and linearized by modifying the approach of [27], is transformed into a heat conduction type of form. The GITT developed by Özisik [28] is employed to obtain analytical solutions describing fluctuations in the groundwater level.

The key conclusions are summarized as follows.

(1) Model validation**:** The proposed analytical solution shows strong agreement with the results of [15] under fixed boundary water levels, with only minor discrepancies observed at extended simulation times, affirming the model's accuracy.

(2) Convergence efficiency**:** When compared with the Laplace-transform-based solutions in [15], the GITT achieves faster convergence, especially under small slope conditions. This efficiency becomes increasingly significant in large-scale or real-time applications.

(3) Effects of recharge and hydraulic properties**:** The influence of uniform and time-variable surface recharge on groundwater dynamics was analyzed separately. Under uniform recharge, increasing the slope reduces groundwater levels due to enhanced flow velocities. Hydraulic conductivity has a pronounced effect on peak groundwater levels, where higher values lower peak levels and hasten the system's stabilization.

(4) Temporal recharge patterns**:** Time-variable recharge was modeled using unit step functions. Three recharge patterns (early peak, central peak, and double peak) were compared under identical recharge volumes. Higher hydraulic conductivity leads to faster drawdown post-recharge, and greater slopes reduce the peak water levels while shifting them downstream. The magnitude and timing of recharge critically influence the spatial and temporal distribution of groundwater dynamics.

(5) Impact of leakage**:** Vertical leakage becomes increasingly significant under rising boundary conditions and low aquifer conductivity. Although slope angle has a lesser impact, the contrast

between the conductivity of the aquifer and of the leakage layer strongly influences the leakage rate.

These findings underscore the importance of incorporating both the variability of recharge and leakage characteristics when modeling groundwater for accurate prediction and sustainable water management in complex hydrogeological environments.

Author contributions

Siao-Ya Tang: Writing – original draft, writing – validation, methodology, investigation, formal analysis; Ping-Cheng Hsieh: Writing – review and editing, methodology, investigation, conceptualization, resources, funding acquisition. All authors have read and approved the final version of the manuscript for publication.

Use of Generative AI tools declaration

While preparing this work, the authors used Chat-GPT and Grammarly for English editing to improve language and readability. After using this tool/service, the authors reviewed and edited the content as needed, taking full responsibility for the publication's content.

Acknowledgments

The National Science and Technology Council of Taiwan financially supported this study under Grant No. NSTC 112-2313-B-005-012.

Conflict of interest

The authors declare that they have no known competing financial interests or personal relationships that could have appeared to influence the work reported in this paper.

References

1. M. A. Marino, Rise and decline of the water table induced by vertical recharge, *J. Hydrol.*, **23** (1974), 289–298. https://doi.org/10.1016/0022-1694(74)90009-2
2. S. Ram, H. S. Chauhan, Analytical and experimental solutions for drainage of sloping lands with time-varying recharge, *Water Resour. Res.*, **23** (1987), 1090–1096. https://doi.org/10.1029/WR023i006p01090
3. N. E. C. Verhoest, P. A. Troch, Some analytical solutions of the linearized Boussinesq equation with recharge for a sloping aquifer, *Water Resour. Res.*, **36** (2000), 793–800. https://doi.org/10.1029/1999WR900317
4. T. S. Zissis, I. S. Teloglou, G. A. Terzidis, Response of a sloping aquifer to constant replenishment and to stream varying water level, *J. Hydrol.*, **243** (2001), 180–191. https://doi.org/10.1016/S0022-1694(00)00415-7
5. C. J. Hung, P. W. Chang, Y. C. Tan, C. H. Chen, Response effect on layer aquifers with hill slope to replenishment, *J. Taiwan Water Conserv.*, **50** (2002), 27–41. (in Chinese)

6. I. S. Teloglou, R. K. Bansal, Transient solution for stream–unconfined aquifer interaction due to time varying stream head and in the presence of leakage, *J. Hydrol.*, **428-429** (2012), 68–79. https://doi.org/10.1016/j.jhydrol.2012.01.024
7. R. K. Bansal, Analytical solution of linearized Boussinesq equation for unsteady seepage flow in ditch-drain sloping aquifer, *J. Hydrogeol. Hydrol. Eng.*, **3** (2014). https://doi.org/10.4172/2325-9647.1000115
8. C. J. Hung, Y. C. Tan, C. H. Chen, J. M. Chen, P. W. Chang, Analytical solution of water table fluctuations above an inclined leaky layer due to ditch recharge, *Hydrol. Process*., **20** (2006), 1597–1609. https://doi.org/10.1002/hyp.5947
9. R. K. Bansal, Groundwater flow in sloping aquifer under localized transient recharge: Analytical study, *J. Hydraul. Eng.*, **139** (2013), 1165–1174. https://doi.org/10.1061/(ASCE)HY.1943-7900.0000784
10. R. K. Bansal, C. K. Lande, A. Warke, Unsteady groundwater flow over sloping beds: Analytical quantification of stream–aquifer interaction in presence of thin vertical clogging layer, *J. Hydrol. Eng*., **21** (2016), 04016017. https://doi.org/10.1061/(ASCE)HE.1943-5584.0001362
11. X. Liang, Y. K. Zhang, A new analytical method for groundwater recharge and discharge estimation, *J. Hydrol.*, **450-451** (2012), 17–24. https://doi.org/10.1016/j.jhydrol.2012.05.036
12. C. J. Hung, C. H. Chen, Y. C. Tan, The analytical solution of water table with moving boundary on an inclined leaky aquifer, *J. Taiwan Water Conserv.*, **51** (2003), 36–41. (in Chinese)
13. R. K. Bansal, S. K. Das, Effects of bed slope on water head and flow rate at the interfaces between the stream and groundwater: Analytical study, *J. Hydrol. Eng.*, **14** (2009), 832–838. https://doi.org/10.1061/(ASCE)HE.1943-5584.0000048
14. R. Bansal, S. Das, Analytical solution for transient hydraulic head, flow rate and volumetric exchange in an aquifer under recharge condition, *J. Hydrol. Hydromech.*, **57** (2009), 113–120. https://doi.org/10.2478/v10098-009-0010-4
15. R. K. Bansal, S. K. Das, Response of an unconfined sloping aquifer to constant recharge and seepage from the stream of varying water level, *Water Resour. Manage.*, **25** (2011), 893–911. https://doi.org/10.1007/s11269-010-9732-7
16. R. K. Bansal, Groundwater fluctuations in sloping aquifers induced by time-varying replenishment and seepage from a uniformly rising stream, *Transp. Porous Med.*, **94** (2012), 817–836. https://doi.org/10.1007/s11242-012-0026-9
17. R. K. Bansal, Unsteady seepage flow over sloping beds in response to multiple localized recharge, *Appl. Water Sci.*, **7** (2017), 777–786. https://doi.org/10.1007/s13201-015-0290-2
18. G. He, T. Wang, Z. Zhao, Y. Hao, T. J. Yeh, H. Zhan, One-dimensional analytical solution for hydraulic head and numerical solution for solute transport through a horizontal fracture for submarine groundwater discharge, *J. Contamin. Hydrol*., **206** (2017), 1–9. https://doi.org/10.1016/j.jconhyd.2017.08.012
19. A. Upadhyaya, H. S. Chauhan, Water table fluctuations due to canal seepage and time varying recharge, *J. Hydrol.*, **244** (2001), 1–8. https://doi.org/10.1016/S0022-1694(00)00328-0
20. A. Upadhyaya, M. M. Kankarej, Analytical and numerical solutions to describe water table fluctuation due to canal and time-varying recharge, *J. Hydroinform.*, **24** (2022), 932–948. https://doi.org/10.2166/hydro.2022.037
21. P. Shi, J. Liu, Y. Zong, K. Teng, Y. Huang, L. Xiao, Analytical solution for NonDarcian effect on transient confined–unconfined flow in a confined aquifer, *J. Groundw. Sci. Eng.*, **11** (2023), 365–378. https://doi.org/10.26599/JGSE.2023.9280029

22. R. Valois, A. Rivière, J. M. Vouillamoz, G. C. Rau, Analytical solution for well water response to Earth tides in leaky aquifers with storage and compressibility in the aquitard, *Hydrol. Earth Syst. Sci.*, **28** (2024), 1041–1054. https://doi.org/10.5194/hess-28-1041-2024
23. C. Turnadge, R. M. Neupauer, O. Batelaan, R. S. Crosbie, C. T. Simmons, Analytical and numerical adjoint solutions for cumulative streamflow depletion, *J. Hydrol.*, **662** (2025), 133820. https://doi.org/10.1016/j.jhydrol.2025.133820
24. Z. Huang, X. Zhou, H. Wang, Q. Wang, Y. S. Wu, Stress sensitivity analysis of vuggy porous media based on two-scale fractal theory, *Sci. Rep.*, **14** (2024), 20710. https://doi.org/10.1038/s41598-024-71171-2
25. S. Yang, R. Cui, X. Yuan, M. Zou, Fractal study on permeability characteristics in rough and dense porous media, *Chem. Eng. Sci.*, **282** (2023), 119265. https://doi.org/10.1016/j.ces.2023.119265
26. G. Li, Y. Yang, X. Cao, S. Zhang, Q. Lv, Y. Su, et al., The fractal analysis of the forced imbibition process in roughened porous media with slip length, *Phys. Fluids*, **37** (2025), 046603. https://doi.org/10.1063/5.0257435
27. J. Bear, *Dynamics of fluids in porous media*, New York: Elsevier, 1972.
28. M. N. Özisik, *Boundary value problems of heat conduction*, New York: Dover Publications Inc., 1968.
29. E. C. Childs, Drainage of groundwater resting on a sloping bed, *Water Resour. Res*., **7** (1971), 1256–1263. https://doi.org/10.1029/WR007i005p01256

AIMS Press